Accepted manuscript of: A. Awadelseed, A. Lewicki, C. Odeh and A. Iqbal, "Cascaded Buck Hybrid Interlink Converter for Multiple-Input / Multiple-Output Operation," 2024 4th International Conference on Smart Grid and Renewable Energy (SGRE), Doha, Qatar, 2024, pp. 1-7, doi: 10.1109/SGRE59715.2024.10428124.

Cascaded Buck Hybrid Interlink Converter for Multiple-Input / Multiple-Output Operation

Ahmed Awadelseed
Faculty of Electrical and Control Engineering, Gdansk University of Technology,
Gdansk, Poland
ahmed.awadelseed@pg.edu.pl

Arkadiusz Lewicki
Faculty of Electrical and Control Engineering, Gdansk University of Technology,
Gdansk, Poland
arkadiusz.lewicki@pg.edu.pl

Charles Odeh
Faculty of Electrical and Control Engineering, Gdansk University of Technology,
Gdansk, Poland
charles.odeh@pg.edu.pl

Atif Iqbal
Department of Electrical Engineering, Qatar University
Doha, Qatar
atif.iqbal@qu.edu.qa

***Abstract*— The provision of isolated- and non-isolated DC output voltages by Power electronics power-conditioning devices in the recent 'green-energy-revolution' era is on course. In this paper, a structure for multi-input multi-output (MIMO) DC–DC buck converter is proposed to generate output voltages of varying levels with fewer component-count. The DC output voltage of each of the constituting buck converters can be used independently or cascaded with one another, depending on the output load voltage requirement. The converter operational modes are analysed and its gain models are derived. Also, expressions for the efficiency and power density of the proposed buck converter are presented. Distinct features of proposed converter are: its simplified configuration, high input/output power density, low-cost involvement, reduction of ripple amplitudes of the source currents, and possibility of deploying energy sources with different voltage-current characteristics. High voltage gain, and bidirectional power flow can be achieved in the converter operations. Experimental results on a laboratory prototype of the proposed MIMO validated the presented DC-DC buck converter topological concept.**

***Keywords*—**DC-DC buck converter, isolated converter, MIMO converter.

I. Introduction

In order to increase the reliability of the power conversion systems, several energy supplies have to be applied in renewable energy sources. Multiple ports with various voltage levels are becoming attractive candidate for interfacing renewable energy conversion systems and electrical vehicle applications; due to its ability to mitigate intermittency issues associated with these energy sources [1]. Recently, multi-input/output ports converters were used in large scales for various portable applications which have: less components, light weight, low cost, and high efficiency performances, [2]. A typical layout of MIMO showing the different possible applications is shown in the Fig. 1.

Multiple port converters play a vital role in integrating and interfacing energy sources with the loads. Generally, multiple port converters can be classified into isolated and non-isolated topologies. Each group can be further

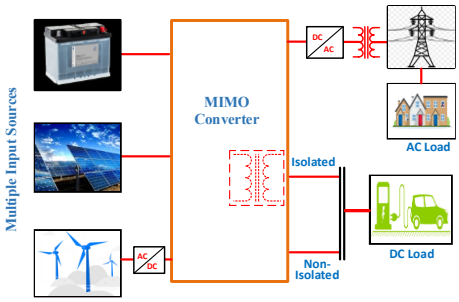

Fig. 1. A typical layout representing a MIMO based applications.

classified as single-input, multi-output (SIMO), [4]-[6]; multi-input single output (MISO), [7]-[9]; and multi-input multi-output (MIMO), [10]-[18] converters. Multiple-port converters can be configured by using a combination of several single-input, single-output (SISO) converters that are connected to a common DC bus. But the main drawback of these configurations is its complex structure and high cost, [3].

In SIMO and MISO, there are more switches required for low- and high-power applications and their control schemes are extremely complicated. Thus, to overcome the drawbacks of these topologies, multiple-input/ multiple-output configurations have been developed. In [4], single-input/multiple-outputs (SIMO) synchronous DC-DC converter was presented. This topology requires four active switches to deliver the multiple output voltages; but has the inherent drawback of many inductors. This increases the cost and bulkiness of the system. Modelling, design and control of two-output buck converter was presented in [5] (with bidirectional/unidirectional power flow capability) for motor drive systems. This structure has high efficiency, low losses, and less component-count. However, it requires power switches with high nominal current; this incurs high costs. A novel integrated synchronous buck DC-DC converter for electric vehicles power supply system was proposed in [6]. Therein, in order to obtain N-ports, N-switches are required. In [7]-[9], bi-directional SIMO buck converters for electric vehicles, PV system and DC nano-grid applications have been developed. The proposed converters produce three output DC voltage ports from single input port; but these topologies have non-isolated

output. Also, they use large number of power switches and inductors; and produce large ripples and high switching losses. In effect, the efficiency of these converters is very low. Moreover, sensitivity of the output voltage to duty ratio variations is among the distinct drawbacks of these converter configurations.

From the aforementioned, it is obvious that SIMO and MISO topologies so far developed have low reliability, poor efficiency and high-cost involvements. To overcome these limitations, multi-input, multi-output (MIMO) converters are configured to generate output voltages with various levels. The topological approach is to combine different input sources, with varying voltage–current characteristics, in a single-stage power conversion. This leads to reduced cost and complexity of the converter; and provides a converter with higher power density. Also, MIMO ensures a smooth distribution of power between the different loads by dividing the currents from all sources. This ultimately distributes the powers accordingly. Some MIMO converters are presented for low power applications, such as wireless sensor networks, [10] and [11].

Among the available MIMO converters, single-inductor MIMO converters are more attractive solution than that of multi-inductor MIMO converters. This is because of their small size, less electromagnetic interference, and low production costs. However, single inductor MIMO requires complicated control techniques to ensure proportional power sharing, [12]. In [13], a simple and effective topology derivation principle, that requires less steps for buck, boost, buck boost converter, was explained in detail. A bipolar DC-DC converter for DC microgrid was presented in [14]. In this configuration, PV module and battery system were integrated using conventional bipolar DC microgrid. However, this topology requires large number of independent DC-DC converters to interface various sources and loads; this increases the cost and decreases the efficiency of the system.

MIMO converters are classified into two types: isolated and non-isolated DC-DC converters. The advantage of non-isolated converter is that it has a more compact design and higher power density than the former; and are better suited to non-isolated applications, [15]-[16]. Isolated DC-DC converters employ transformer-based magnetic coupling. This structure provides isolation between the output and input ports; and improves the voltage gain through turns-ratio of the isolating transformer, [17]-[18].

In this paper, MIMO based on Cascaded-Buck Hybrid Interlink converter (CBHIC) is proposed with dual input DC sources. The presented topology includes four non-isolated DC output ports and two isolated output ports. The proposed CBHIC is shown in Fig. 2; where two series-connected DC sources (V_{S1} and V_{S2}) are used. The DC source V_{s1} is used to supply two buck converters. The outputs of these converters are available at the ports-1 and -2. Also, two buck converters supplied by $V_{S2,}$ and their corresponding outputs are available at ports-3 and -4. The common bus, *com* has less potential than the potential of positive buses $+v_{o1}$ and $+v_{o2}$; and more than the potential of negative buses $-v_{o3}$ and $-v_{o4}$. To achieve boosted output

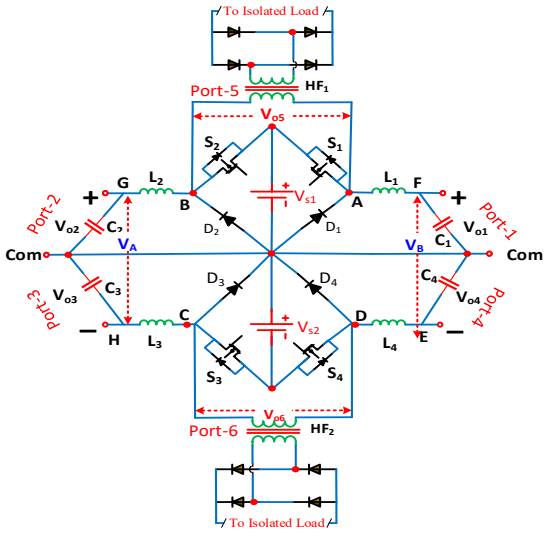

Fig. 2. Schematic of proposed multiport CBHIC.

voltage, the load can be connected between the higher positive and lower negative terminals in (port-1+port-4) and (port-2+port-3) to obtain V_A and V_B, respectively. To ensure the operation of buck-converter in the continuous conduction mode (CCM) and minimize the magnitude of ripple in inductor current, the inductance of the inductor should be high based on factors such as: the desired level of ripples, the frequency of operation, and the size and cost constraints of the converter. Similarly, the capacitance of filter capacitor of buck-converter-1 should be high to keep the ripple amplitude within the defined limit.

The switches S_1 and S_2 are operated in complementary mode to ensure safe commutation of the high-frequency AC current in the primary side of HF-1. As a result, high-frequency AC voltages are present between nodes A and B, as well as between nodes C and D. These AC outputs can be converted into isolated DC outputs using rectifiers connected to transformers HF-1 and HF-2. The outputs at port-5 and -6 can be used to supply power to loads requiring galvanic isolation. Depending upon operational choice, isolated DC outputs available at port-5 and port-6 can be connected in series. The main features of proposed converter in contrast to existing converters are:

1. The topology has inherent low-ripple current source, which makes it suitable for renewable energy application (such as PV panels and fuel cells).
2. It requires four inductors for the combination of four converters. Therefore, cross-regulation issues and sophisticated design techniques are not required to control the converter. Input can be ESS (Energy Storage System), RES (Renewable Energy System) or DC distributed grid to achieve four DC output and two AC output ports.

II. Operational Principle

This section provides the various operational modes of the proposed MIMO-CBHIC, their associated switching states, and the direction of current flow during each mode of operation. In this study, continuous conduction mode (CCM) operation is assumed in the analyses of the proposed topology.

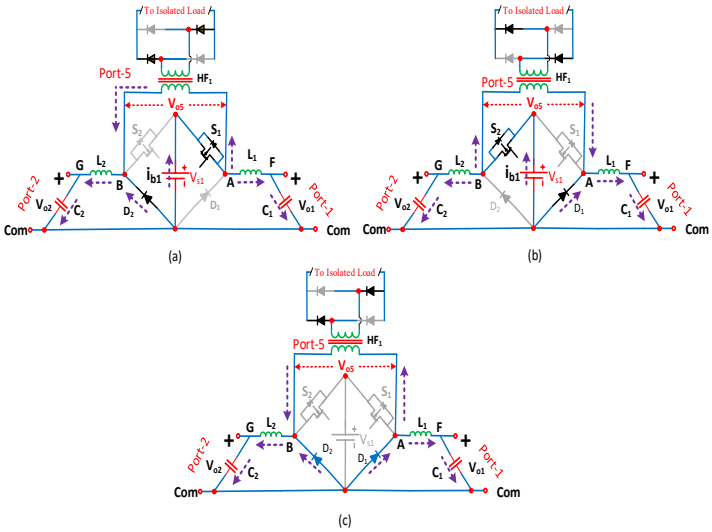

Fig. 3. Equivalent circuit of CBHIC during (a) Mode-I (b) Mode-II (b) Mode-III

A. Mode-I $[t_1\text{-}t_2]$:

Fig. 3(a) shows the equivalent circuit of the proposed converter in mode-I operation. In this mode of operation switch S_1 is turned ON while switch S_2 is OFF. V_{S1} supplies inductors L_1 and D_1 is reverse biased. The output capacitors C_1 discharge through the load connected to output port-1 (non-isolated). Furthermore, the isolated port detects a current route via S_1 and L_2. For this mode, the instantaneous voltage (Fig.4) can be expressed as:

$$v_{o5} = \{(v_{o1} + v_{o2}) + (v_{L1} + v_{L2})\} \tag{1}$$

B. Mode II $[t_4 - t_5]$:

In this mode, switch S_2 is turned ON while S_1 remain OFF as illustrated in Fig. 3(b). Similar to traditional DC-DC buck converter, the inductors L_1 discharge to the loads at port-1, while the capacitors C_2 supply the load demand at port-2. The instantaneous voltage across isolated port-5 can be written as (Fig. 4)

$$v_{o5} = -\{(v_{o1} + v_{o2}) + (v_{L1} + v_{L2})\} \tag{2}$$

C. Mode III: $[(t_0 - t_1), (t_3 - t_4), (t_5 - t_6)]$

This mode is an additional representation of the state that exists in the converter when none of the switches are switched ON (Fig. 4). The conduction is presented in Fig. 3(c), the output voltage at this mode $v_{o5=0}$. During this mode, the inductors (L_1, L_2) will transfer power to the load while maintaining a low ripple output voltage with the aid of an output capacitor. Fig. 4 displays the waveforms of the HF-1 primary voltage (v_{o5}), primary current (i_{p1}) and the gate pulses.

D. Current and Voltage Ripples

Selection of inductor and capacitor is vital in the design of MIMO converters. The voltage across the inductor L_1 (and L_2) is $(v_S - v_{o1})$, (and $(v_S - v_{o2})$), the inductor current can be defined as:

$$\frac{di_{L1/2}}{dt} = \frac{v_s - v_{o1/2}}{L} \tag{3}$$

and the current ripples can be determined using

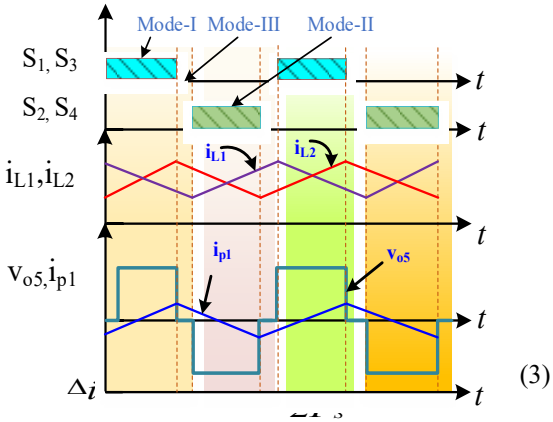

(3)

The minimum value of inductance can be calculated as

$$L = \frac{v_S - v_{o1/2}}{\Delta i_{L1/2}} \frac{D_1}{2T_S} \tag{4}$$

The output capacitor in MIMO is responsible for filtering the output voltage and reducing output voltage ripple. The value of the output capacitor depends on the output current and the desired output voltage ripple. In continuous current mode (Fig. 3), the currents I_{L1} (and I_{L2}) are delivered to both capacitors and the capacitors are discharged continuously on the load side.

E. Voltage Gain of Proposed Converter

The gains of non-isolated buck converter-1 and converter-2 are given by.

$$\frac{v_{o1}}{v_S} = D_1, \frac{v_{o2}}{v_S} = D_2 \tag{5}$$

Here, D_1 is the duty cycle during mode-I operation, and D_2 is duty interval during mode-II operation. In same way, the voltage gains of buck conveter-3 and conveter-4 included in this topology can be calculated.

The voltage gain of isolated ports can be expressed as;

$$\frac{v_{o5}}{v_S} = \frac{D_1}{D_2}, \ \frac{v_{o6}}{v_S} = \frac{D_1}{D_2} \tag{6}$$

It can be observed that, two of three outputs: port-1, port-2, and port-5 can be controlled independently.

III. Simulation Study

In order to prove the feasibility of the proposed CBHIC DC-DC converter, a simulation model has been developed in PLECS environment. The operating frequency is set to 5 kHz, and the input dc voltages are $V_{dc1} = V_{dc2} = 100V$.

A. Modulation Scheme and Control

Fig. 5 shows the block diagram needed to create the necessary switching for the switches used in CBHIC. As shown in Fig. 4(a), the duty cycle needed for switch S_1 is generated by comparing the modulating signal, M_a, with the carrier signal, Vc_1, while the duty cycle for switch S_2 is generated by comparing M_b with Vc_2. The switches S_1 and S_2 operate complementarily, which results in the inductor L_1 and L_2 in adjacent buck converters experiencing simultaneous charging and discharging actions. By adjusting the magnitude of modulation indexes (M_a, M_b), various duty ratios can be achieved. By employing this modulation scheme, we are able to control the output of

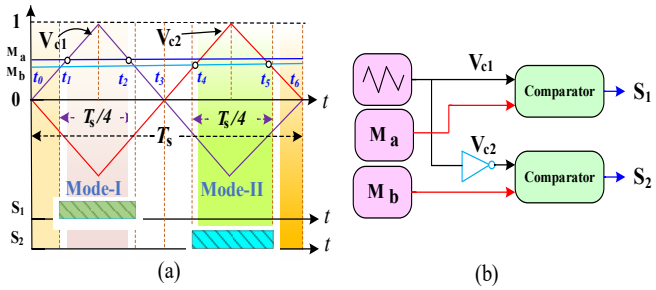

Fig. 5. Generation of a controlling signal and graphical representation of the relationship between duty ratio and modulating signal

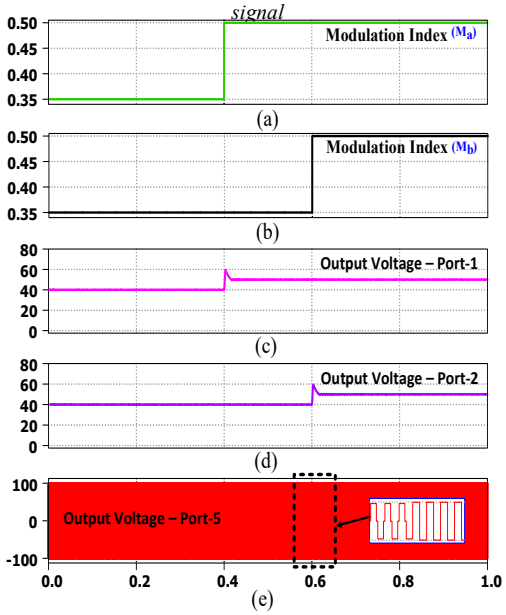

Fig. 6. Steady state waveforms. a) Change in M_a from 0.3 to 0.49.b) Change in M_b from 0.3 to 0.49. c) voltage at port 1 (v_{o1}). d) voltage at port 2 (v_{o2}). e) voltage at port 5 (v_{o5}).

two of three ports separately. Fig. 6(a) to (d) show the output voltages for ports 1, 2, and 5. The result shows the output voltages at port-1, port-2 and port-5 when duty ration changed from 0.35 to 0.49 for converter-1 and converter-2. At the port-1/2 for the two duty cycles, output voltages of 40.V and 50.4V are achieved, while a high voltage of 94.4V and 98V is provided at port-5. Changing the modulation indexes of ports -1-and 2 causes a change in the output voltage on port-5. Due to the converter topology - two of three output ports can be controlled independently. To transfer energy from input to output ports, switch S_1 must be turned on to obtain output voltage at port-1, switch S_2 must be turned on to acquire output voltage at port-2, and both switches (S_1, S_2) must be used to get voltage at port-5.The pulses for switches (S_1, S_2), inductor current (i_{L1}, i_{L2}) voltage across port-5 and source current (i_{b1}) are presented in Fig. 7. During the OFF state of the switches, the inductor current decreases and delivers its energy into capacitors. The nature of inductor current is continuous.

Online load variations are used to assess the dynamic response of a converter design. Fig.8 depicts the change in load at port-1 and port-2 at 0.2sec and 0.4sec respectively, while the load at port-5 is changed at 0.6sec. The load current at port-1(i_{o1}) changed from 1.43 A to 3.033 A, while the load current at isolated port (port-5) changed

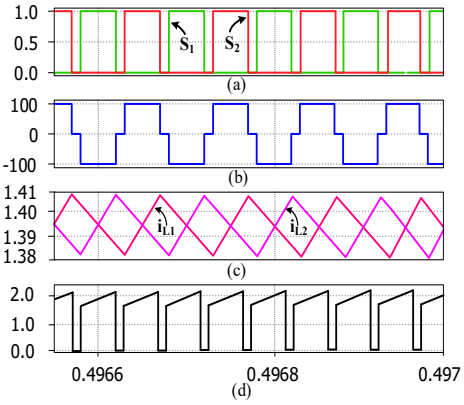

Fig. 7. Simulation result. a) Gate pulses (S_1,S_2). b) Output voltage (v_{o5}). c) inductor currents (i_{L1} , i_{L2}). d) input source current (i_{b1}).

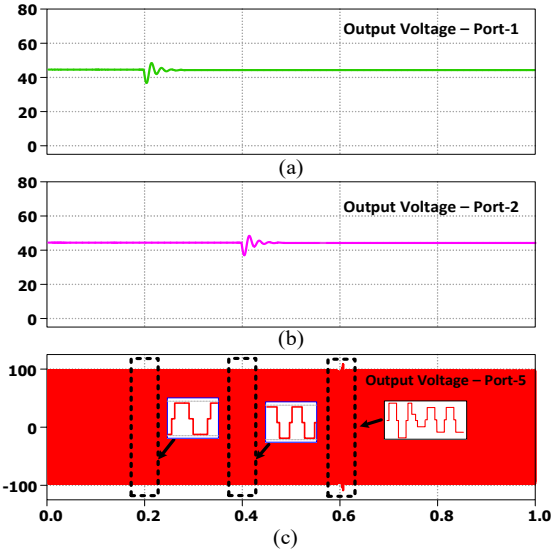

Fig. 8. Simulation results of output voltages. a) voltage at port 1 (v_{o1}). b) voltage at port 2 (v_{o2}). c) voltage at port 5 (v_{o5}).

from 0.97 A to 3.152 A. It can be observed that the load change on the output ports (isolated/non-isolated) have no influence on the rest of ports.

B. Efficiency and Power Density of CBHIC

To evaluate the efficiency of the proposed CBHIC, the losses occurring in the converter due to the non-ideal behavior of various elements of CBHIC are calculated. By using the output power delivered by the CBHIC and the losses, occurring in the CBHIC, the efficiency 'η' evaluation of CBHIC can be carried out.

$$\eta = \frac{P_o + P_{iso}}{P_s} = \frac{\sum_{i=1}^{4}(V_{oi}\times I_{oi}) + \frac{1}{2}\sum_{i=1}^{2}(V_{si}\times I_{si})}{(V_{s1}+V_{s2})(i_{b1}=i_{b2}) + P_{sw}} \qquad (7)$$

where P_{iso} is the isolated port power, P_{sw} are the switching looses, P_s is the source power.

Now the efficiency of the CBHIC is evaluated using the analytical method given by (7) and using the simulation in PLECS software. PLECS provides the facility for thermal modelling of power electronics devices and is used for accurate measurement of power losses occurring in various elements of the dc-dc converters. The thermal model of the proposed MIMO converter was created with PLECS software utilizing the available data of IKW75N60T switches. The load parameters were modified to determine

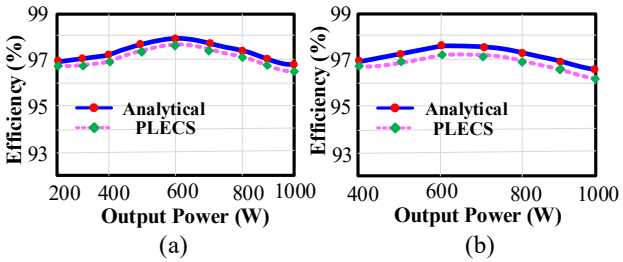

Fig. 9. Efficiency of the CBHIC (a) when the load demand at non-isolated ports is varied (b) when load demand at isolated ports is varied.

the efficiency at the output ports. Fig. 9(a) shows how efficiency fluctuates as non-isolated port loads vary from 0W to 600W, while isolated ports maintain a constant 200W load. In Fig. 9(a), CBHIC efficiency peaks at 600W before declining due to lower losses at reduced loads.

A dotted-line graph in PLECS measures this efficiency fluctuation. The Fig. 9(b) displays CBHIC efficiency as isolated port loads vary from 0W to 600W, while non-isolated ports maintain a constant 400W load. Non-isolated ports 1, 2, 3, and 4 have a 400W initial load, while isolated ports 5 and 6 range from 0W to 600W. The efficiency graphs in Fig. 9 reveal minimal impact from cascading CBHICs on converter efficiency, confirming agreement between analytical and simulation results.

IV. Comparison of Proposed Converter with State of Art DC-DC Converters

The state-of-the-art MIMO-based DC-DC converters described in the literature are compared to the proposed MIMO-CBHIC in this section. In Table I, comparison between the proposed topology and existing configurations are given in terms of voltage gain, efficiency, voltage stress across switches and diodes, number of input ports, number of output ports (isolated and non-isolated), and component count. It can be observed that the voltage gain of the proposed MIMO converter and DC-DC converters suggested in [4], [6] are identical and equal to conventional DC-DC buck converters. In [4], three output ports are achieved and they work dependently; this converter configuration requires high number of components to generate single isolated port which make the system bulky and complex control technique was used in generating the switching pulses. In [6], it is only possible to get two non-isolated output ports. The number of components used in this topology are high, which leads to increased cost, losses and overall reduction in efficiency and requires additional balancing circuit to control the voltage across capacitors. Single isolated output port was achieved using configurations proposed in [17], [19], and [20]. However, the topology presented in [20] has a small range of load voltage variation and the control technique increases the losses in the converter. In all these topologies, the number of elements is not fully optimized to get high number of output ports, extra inductors and floating drivers are needed for some switches. In contrast to previous similar configurations, lower cost and higher power density can be achieved using the proposed topology. No additional voltage-balancing control is required; thus, reducing the complexity of the control.

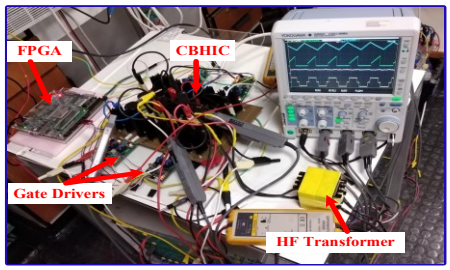

Fig. 10. Lab prototype of CBHIC

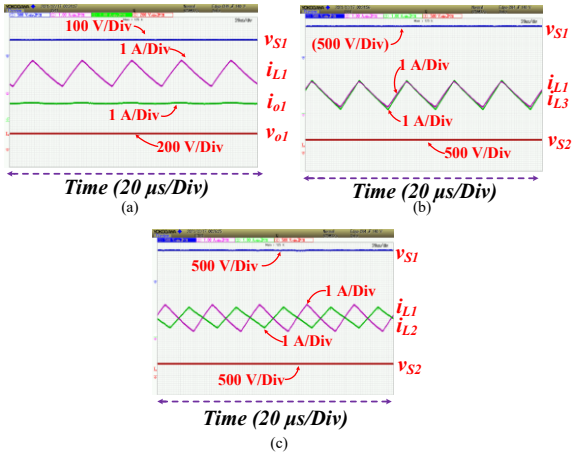

Fig. 11. (a) source-1 voltage, inductor L_1 current, inductor L_2current, source-2 voltage. (b) source-1 voltage, inductor L_1 current, inductor L_3 current, source-2 voltage. (c) source-1 voltage, inductor L_1 current, load current of converter-1, output voltage of converter-1.

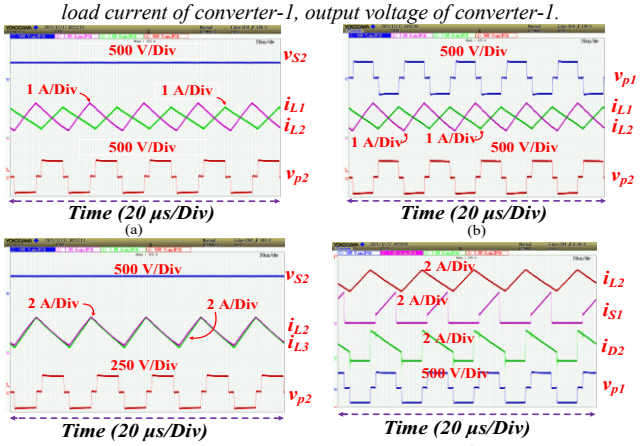

Fig. 12. Experimental waveforms of: (a) source-2 voltage, inductor L_1 current, inductor L_2 current, primary voltage of HF-2. (b) primary voltage of HF-1, inductor L_1 current, inductor L_2 current, primary voltage of HF-2. (c) source-2 voltage, inductor L_1 current, inductor L_2 current, primary voltage of HF-2. (d) inductor L_2 current, S_1 transistor current, diode D_2 current, primary voltage of HF-1

V. Experimental Validation

A laboratory prototype of the proposed converter (400 W rated) was built to verify the effectiveness and topological concept of the proposed converter as shown in Fig. 10. The prototype includes MOSFETs (C3M0065090D), and Schottky diode (STTH30R04W) was selected as the freewheeling diode. The capacitors and inductors are selected to be 180µF and 120µH, respectively. Switching frequency of 50 kHz was used. The loads connected at the output terminals of the converters are resistive load.

Fig. 11(a) shows the experimental waveforms of the inductor currents for converter-1 (i_{L1}), converter-2 (i_{L2}) and

TABLE I. COMPARISION OF MIMO DC-DC CONVERTERS

Topology	Voltage Gain (G)	Number of input ports	Number of output ports		Number of elements	Control/Hardware Complexity	Voltage stress		Efficiency (%)
			Non- isolated	Isolated	C/I/D/S/T		Diode	Switches	
[4]	$G_1 = d_1$ $G_2 = (1-d_2)$ $G_3 = (1-d_3)$	1	3	-	3/3/0/4/10	Output is unidirectional connected directly to dc bus, high ripple in source current.	-	$S_{1,2,3,4} \rightarrow \frac{v_o}{2v_s}$	92.4
[6]	d	2	-	1	5/6/4/3/18	Output is bidirectional, limitation to getting maximum power from the inputs.	$D_{1,2,3,4} \rightarrow \frac{v_s - v_o}{v_s}$	$S_1 \rightarrow v_s$ $S_2 \rightarrow \frac{1-v_o}{v_s}$	94.5
[17]	$G_1 = d_1, G_2 = d_2$	1	2	-	2/2/0/4/8	Output is bidirectional, extra inductors, Complex control.	-	$S_{1,2} \rightarrow v_s$	91.4
[19]	$G_1 = \frac{d_1(1+d_1-d_2)}{(1-d_1)}$ $G_2 = -\frac{d_2}{(1-d_2)}$	2	2	-	6/3/4/3/12	Output is bidirectional, additional decoupling capacitor required, and wide ripple on input currents.	$D_{1,3} \rightarrow v_S$ $D_{2,4} \rightarrow v_S - v_o$	$S_{1,2} \rightarrow v_s$ $S_3 \rightarrow \frac{v_s - v_o}{v_s}$	93.9
[20]	$G = \frac{d}{(1-d)}$	2	-	1	4/4/2/6/16	Output is unidirectional, high number of gate drivers. additional voltage balance control. high ripple in source current.	$D_{1,2} \rightarrow v_S$	$S_{1,2,5} \rightarrow v_s$ $S_{3,4} \rightarrow \frac{v_s - v_o}{v_s}$	96.4
[P]	$G_1 = d_1, G_n = nd_1$	**2**	**4**	**2**	**4/4/4/4/16**	Less nnumber of gate drivers, simple control technique, low source current ripple.	$D_{1,2,3,4} \rightarrow v_S$	$S_{1,2,3,4} \rightarrow v$	**97.4**

C=Number of capacitors, I= Number of inductors, D=number of diodes, S= Number of switches, T= Total device count, G= Voltage gain, d_1, d_2, d_3= duty cycles

the input voltages for the whole converters (V_{s1}, V_{s2}). Therein, when the charging action of inductor L_1 is taking place, the inductor L_2 is being discharged through the load and output capacitor C_{o2}. The average values of these currents are 4.42A and 4.30A respectively. The source voltages are selected to be each 400 V (V_{s1}=V_{s2} =400V). The corresponding inductor currents for converter-1 and converter-3 are shown in Fig. 11(b). It can be observed that the inductor currents for converter-1 and -3 (i_{L1}, i_{L2}) are identical with average values of 4.51 A and 4.36 A, respectively. Fig. 11(c) shows the waveform of input voltage inductor current i_{L1}, converter-1 output voltage (v_{o1}) and load current (i_{o1}). The duty cycles of the buck converters 1, -2, -3 and -4 were maintained at a value of 0.45. The average value of output voltage v_{o1} is 162.5V and load current $i_{o1}$is 2.4A.

For high frequency AC output ports, Fig. 12 shows the experimental waveforms for different source voltages, output voltages, transistor currents, output currents, primary, secondary voltages of transformers HF-1 and HF-2, and the DC-DC buck converter voltages and currents. Fig. 12(a) shows the waveforms of source voltage v_{S1}, inductor currents (i_{L1}, i_{L2}) and voltage applied to primary of HF-2 (v_{p1}). It is observed that charging and discharging action of inductors L_1 and L_2 are in phase opposition. It is due to the complementary action of switches (S_1, S_2). The primary voltages of HF-1 and HF-2 (v_{p1}, v_{p2}) and inductor currents (i_{L1}, i_{L2}) are presented in Fig. 12(b). The primary voltages (v_{p1}, v_{p2}) of HF-1 and HF-2 are observed to be 180^o out of phase due to the complementary action of switches S_1 and S_4. Fig. 12(c) displays the source voltage (V_{s1}), primary voltage of transformer HF-1 (v_{p1}) and inductor currents (i_{L1}, i_{L3}). Also, the waveforms of source current (i_{S1}), diode-2 current (i_{D1}) and inductor current (i_{L2}) are shown. The peak value of the primary voltage of HF-1 is 400V.

VI. CONCLUSION

Presented in this paper is a MIMO based DC-DC buck converter, CBHIC. There are two input ports and six output ports on the CBHIC. Four of the six output ports are non-isolated, while the other two are isolated. The evaluated efficiency of CBHIC is comparable to the DC-DC converter topologies recently reported in the literature. As a result, it is a suitable solution for a variety of applications that require isolated and non-isolated DC supply, such as electric vehicles (EVs). However, it should be noted that only two of the three ports in each part of the converter can be controlled independently. The complementary actions of switches in the CBHIC decrease the ripple amplitudes in the source currents; this lowers the filtering element values. Experimental results obtained from a laboratory prototype validated the topological and operational concepts of the MIMO-CBHIC. At 600 W rated output power, the converter has 97.4 % efficiency.

REFERENCES

[1] S. R. Khasim, C. Dhanamjayulu and S. M. Muyeen, "A Single Inductor Multi-Port Power Converter for Electric Vehicle Applications," in IEEE Access, vol. 11, pp. 3367-3385, 2023, doi: 10.1109/ACCESS.2023.3234105.

[2] S. Dusmez, X. Li and B. Akin, "A New Multiinput Three-Level DC/DC Converter," in IEEE Transactions on Power Electronics, vol. 31, no. 2, pp. 1230-1240, Feb. 2016, doi: 10.1109/TPEL.2015.2424246.

[3] V. A. K. Prabhala, P. Fajri, V. S. P. Gouribhatla, B. P. Baddipadiga and M. Ferdowsi, "A DC–DC Converter with High Voltage Gain and Two Input Boost Stages," in IEEE Transactions on Power Electronics, vol. 31, no. 6, pp. 4206-4215, June 2016, doi: 10.1109/TPEL.2015.2476377

[4] B. K. Sabbarapu, O. Nezamuddin, A. McGinnis and E. dos Santos, "Single-input multiple-output synchronous DC-DC buck converter," 2016 IEEE Energy Conversion Congress and Exposition (ECCE), Milwaukee, WI, USA, 2016, pp. 1-8, doi: 10.1109/ECCE.2016.7855438.

[5] Euzeli Cipriano dos Santos, "Dual-output dc-dc buck converters with bidirectional and unidirectional characteristics," IET Power Electron., 2013.5, (6), pp. 999-1009 (doi: http://doi.org/10.1049/iet-pel.2012.0731).

[6] M. Ramesh, B. Mallikarjuna and T. Rajasekar, "A Novel Investigation on Single-Input Three-Output DC-DC Buck Converter for Electrical Vehicles," 2021 7th International Conference on Electrical Energy Systems (ICEES), 2021, pp. 141-146, doi: 10.1109/ICEES51510.2021.9383635.
[7] J. Zeng, W. Qiao and Liyan Qu, "An isolated three-port bidirectional DC-DC converter for photovoltaic systems with energy storage," 2013 IEEE Industry Applications Society Annual Meeting, 2013, pp. 1-8, doi: 10.1109/IAS.2013.6682520
[8] G. Chen, Y. Deng, J. Dong, Y. Hu, L. Jiang and X. He, "Integrated Multiple-Output Synchronous Buck Converter for Electric Vehicle Power Supply," in IEEE Transactions on Vehicular Technology, vol. 66, no. 7, pp. 5752-5761, July 2017, doi: 10.1109/TVT.2016.2633068.
[9] I. Askarian, M. Pahlevani and A. M. Knight, "Three-Port Bidirectional DC/DC Converter for DC Nanogrids," in IEEE Transactions on Power Electronics, vol. 36, no. 7, pp. 8000-8011, July 2021, doi: 10.1109/TPEL.2020.3046453.
[10] A. Elshora and H. A. Gabbar, "Design and Analysis of Multi-Input, Single-Output, Nonisolated DC/DC Converter for Fast Charging of Electric Vehicles," 2021 International Conference on Electrical, Computer, Communications and Mechatronics Engineering (ICECCME), 2021, pp. 1-7, doi: 10.1109/ICECCME52200.2021.9591071.
[11] Y. Liu and Y. Chen, "A Systematic Approach to Synthesizing Multi-Input DC–DC Converters," in IEEE Transactions on Power Electronics, vol. 24, no. 1, pp. 116-127, Jan. 2009, doi: 10.1109/TPEL.2008.2009170.
[12] Q.Wang, J.Zhang, X.Ruan, K. Jin, "Isolated Single Primary Winding Multiple-Input Converters" IEEE Trans On Power Electronics, Vol. 26, No. 12, Dec2011.
[13] K. Chan et al., "Multiple Input Single Output Converter with Uneven Load Sharing Control for Improved Efficiency," 2021 IEEE Conference on Energy Conversion (CENCON), 2021, pp. 46-51, doi: 10.1109/CENCON51869.2021.9627255.
[14] R. Jain, A. Laddha and N. Satyanarayana, "DC-DC Converter and Its Multiport Interface," 2019 IEEE 16th India Council International Conference (INDICON), 2019, pp. 1-4, doi: 10.1109/INDICON47234.2019.9030313.
[15] K. Nguyen, T. Taufik, R. N. Hasanah and T. Nurwati, "Multiple Input Single Output Converter with MPPT for Renewable Energy Applications," 2020 10th Electrical Power, Electronics, Communications, Controls and Informatics Seminar (EECCIS), 2020, pp. 81-86, doi: 10.1109/EECCIS49483.2020.9263470.
[16] M. Dhananjaya and S. Pattnaik, "Design and Implementation of a Multi-Input Single-Output DC-DC Converter," 2019 IEEE International Conference on Sustainable Energy Technologies and Systems (ICSETS), 2019, pp. 194-199, doi: 10.1109/ICSETS.2019.8744815.
[17] Q. Wang, J. Zhang, X. Ruan and K. Jin, "Isolated Single Primary Winding Multiple-Input Converters," in IEEE Transactions on Power Electronics, vol. 26, no. 12, pp. 3435-3442, Dec. 2011, doi: 10.1109/TPEL.2010.2103958.
[18] M. Azizi, M. Mohamadian and R. Beiranvand, "A New Family of Multi-Input Converters Based on Three Switches Leg," in IEEE Transactions on Industrial Electronics, vol. 63, no. 11, pp. 6812-6822, Nov. 2016, doi: 10.1109/TIE.2016.2581765.
[19] P. Mohseni et al."A New High Step-Up Multi-Input Multi-Output DC–DC Converter," in IEEE Transactions on Industrial Electronics, vol. 66, no. 7, pp. 5197-5208, July 2019, doi: 10.1109/TIE.2018.2868281.
[20] H. Aljarajreh, D. D. -C. Lu, Y. P. Siwakoti and C. K. Tse, "A Nonisolated Three-Port DC–DC Converter With Two Bidirectional Ports and Fewer Components," in IEEE Transactions on Power Electronics, vol. 37, no. 7, pp. 8207-8216, July 2022, doi: 10.1109/TPEL.2022.3146837.